

Compromised Structure and Function of HDAC8 Mutants Identified in Cornelia de Lange Syndrome Spectrum Disorders

Christophe Decroos,[†] Christine M. Bowman,[†] Joe-Ann S. Moser,[†] Karen E. Christianson,[†] Matthew A. Deardorff,^{‡,§} and David W. Christianson^{*,†}

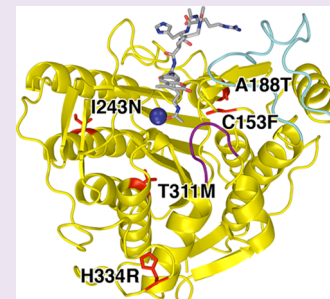
[†]Roy and Diana Vagelos Laboratories, Department of Chemistry, University of Pennsylvania, Philadelphia, Pennsylvania 19104-6323 United States

[‡]Division of Human Genetics and Molecular Biology, The Children's Hospital of Philadelphia, Philadelphia, Pennsylvania 19104 United States

[§]Department of Pediatrics, Perelman School of Medicine, University of Pennsylvania, Philadelphia, Pennsylvania 19104 United States

Supporting Information

ABSTRACT: Cornelia de Lange Syndrome (CdLS) is a multiple congenital anomaly disorder resulting from mutations in genes that encode the core components of the cohesin complex, SMC1A, SMC3, and RAD21, or two of its regulatory proteins, NIPBL and HDAC8. HDAC8 is the human SMC3 lysine deacetylase required for cohesin recycling in the cell cycle. To date, 16 different missense mutations in HDAC8 have recently been identified in children diagnosed with CdLS. To understand the molecular effects of these mutations in causing CdLS and overlapping phenotypes, we have fully characterized the structure and function of five HDAC8 mutants: C153F, A188T, I243N, T311M, and H334R. X-ray crystal structures reveal that each mutation causes local structural changes that compromise catalysis and/or thermostability. For example, the C153F mutation triggers conformational changes that block acetate product release channels, resulting in only 2% residual catalytic activity. In contrast, the H334R mutation causes structural changes in a polypeptide loop distant from the active site and results in 91% residual activity, but the thermostability of this mutant is significantly compromised. Strikingly, the catalytic activity of these mutants can be partially or fully rescued *in vitro* by the HDAC8 activator *N*-(phenylcarbamothioyl)benzamide. These results suggest that HDAC8 activators might be useful leads in the search for new therapeutic strategies in managing CdLS.



Cohesin and its effectors are tightly regulated during essential cellular processes in eukaryotes, such as sister chromatid cohesion in the cell cycle, DNA repair, and gene expression.^{1,2} Cohesin is comprised of four different protein components: SMC1A, SMC3, RAD21, and STAG.² SMC1A and SMC3 are elongated proteins, each of which contains an ATPase head domain at one end and a “hinge” domain at the other end, separated by a long coiled-coil segment. In the cohesin complex, SMC1A and SMC3 associate through their hinge domains and their ATPase domains, which are also stabilized by the binding of RAD21. In other words, SMC1A and SMC3 are analogous to the two half-rings of a hinged bracelet, and RAD21 is the clasp. Finally, STAG binds to RAD21. The overall cohesin complex is thought to adopt a ring-like quaternary structure³ capable of encircling two sister chromatids.^{2–4}

Cohesinopathies are human developmental syndromes caused by mutations in the protein components of the cohesin complex or in the proteins that regulate the function of this complex. Notable cohesinopathies include Cornelia de Lange Syndrome (CdLS), Roberts Syndrome, and Warsaw Breakage Syndrome.^{5–7} Classical CdLS occurs in approximately 1 per 10 000 births and is a genetically heterogeneous disorder characterized by distinctive facial features (synophrys, long eyelashes, upturned nose, thin downturned lips), intellectual

disability, and limb abnormalities such as missing fingers or arms.^{8,9} CdLS results from defects in genes that encode cohesin proteins or mediators of cohesin function. For example, the protein NIPBL is essential for cohesin–chromatin association,^{10,11} and mutations in the gene encoding NIPBL are found in approximately 50–60% of CdLS patients.^{12–14} Other patients with CdLS that have reduced structural anomalies but significant intellectual disability harbor mutations in core components of the cohesin complex, such as SMC1A and SMC3.¹⁵ Mutations in RAD21 also result in a cohesinopathy closely related to CdLS but with notably less cognitive impairment.¹⁶

Sister chromatid cohesion is established through acetylation of SMC3 during S-phase of the cell cycle at two conserved lysine residues in the ATPase domain (Lys105 and Lys106 in human SMC3) by the lysine acetyltransferase ESCO1.^{17–20} To ensure partial sister chromatid separation in prophase and complete separation in anaphase,^{2,21} these acetylated lysines must be deacetylated. In yeast, deacetylation is mediated by Hos1, a deacetylase related to the class I histone deacetylase

Received: May 14, 2014

Accepted: July 21, 2014

Published: July 30, 2014



family.^{22,23} These zinc-dependent deacetylases are also known more broadly as lysine deacetylases because their biological substrates are not limited to histone proteins.^{24–26} In humans, the class I isozyme²⁷ HDAC8 has recently been identified as the SMC3 deacetylase.²⁸ Significantly, missense and nonsense mutations are found in the gene encoding HDAC8 in several patients with features of CdLS.^{28,29} A total of 16 missense mutations throughout the protein structure have been identified to date and each causes partial to complete loss of catalytic activity (Figure 1).

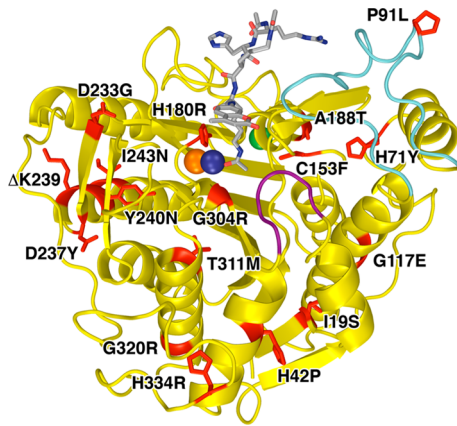


Figure 1. HDAC8 mutations identified in children diagnosed with Cornelia de Lange Syndrome. Mutations (red) are mapped onto the structure of the Y306F HDAC8-substrate complex (PDB 2VSW) (the Y240N mutation is accompanied by the deletion of K239). The assay substrate (Ac-Arg-His-Lys(Ac)-Lys(Ac)-aminomethylcoumarin) is a gray stick-figure and the active site zinc ion is a dark blue sphere. Monovalent cations are shown as orange and green spheres. Purple and cyan segments indicate the L1 and L2 loops, respectively, which can undergo conformational changes to accommodate ligand binding in the active site.

Here, we provide the first view of the molecular basis of compromised HDAC8 function in human developmental disorders. Specifically, we report the structural and functional characterization of five representative HDAC8 mutants identified in CdLS patients, ranging from significantly compromised to nearly fully active enzymes: C153F, A188T, I243N, T311M, and H334R. Additionally, we report the structures of intact enzyme–substrate complexes for certain mutants, thereby enabling comparisons with corresponding HDAC8–substrate complexes.^{30,31} We correlate structural changes with biochemical data to pinpoint structural features that compromise enzyme activity and thermostability, and we demonstrate that compromised catalytic activity can be rescued by an *N*-acylthiourea activator.³²

RESULTS AND DISCUSSION

C153F HDAC8. Among the mutated residues in the current study, Cys153 is closest to the active site and its thiol group is 8 Å from the catalytic Zn²⁺ ion. C153F HDAC8 exhibits only 2% residual catalytic activity relative to the wild-type enzyme, which is the most significant activity loss of the five mutants studied herein (Table 1). Although the overall structure of the C153F HDAC8–SAHA complex is similar to that of the wild-type HDAC8–SAHA complex³³ (root mean square (rms) deviation = 0.48 Å for 358 Cα atoms), the C153F substitution triggers significant local structural changes. Because Phe153 is

Table 1. Catalytic Activities and Melting Temperatures of CdLS HDAC8 Mutants

	activity ^a (nmol product·μmol enzyme ⁻¹ ·min ⁻¹)	melting temp. <i>T_m</i> (°C) ^a	
		no ligand	with M344
wild type	1570 ± 80	50.1 ± 0.1	55.7 ± 0.2
C153F	34 ± 2	48.2 ± 0.1	50.6 ± 0.1
A188T	610 ± 10	46.5 ± 0.1	50.6 ± 0.2
I243N	650 ± 30	40.6 ± 0.1	48.4 ± 0.2
T311M	93 ± 3	42.3 ± 0.1	48.8 ± 0.2
H334R	1430 ± 20	43.1 ± 0.1	50.5 ± 0.2

^aAll measurements made in triplicate and reported as mean ± standard deviation.

too large to be accommodated in the space previously occupied by Cys153, Phe153 is oriented away from the active site and the backbone Cα atom moves 2 Å away from its original position (Figure 2a, Supporting Information Figure S1). In turn, this causes a conformational change for Trp141, which adopts “in” and “out” conformations in the wild-type enzyme: in C153F HDAC8, Trp141 is sterically locked in the “in” conformation by Phe153. These conformational changes permanently block internal channels believed to facilitate release of the product acetate (Figure 2b and c).³⁴

T311M HDAC8. Thr311 is located in helix H2, ~11 Å away from the catalytic Zn²⁺ ion, and T311M HDAC8 exhibits only 6% activity relative to the wild-type enzyme (Table 1). Although the structure of the T311M HDAC8–TSA complex is similar to that of the wild-type HDAC8–TSA complex³³ (rms deviation = 0.68 Å for 360 Cα atoms), the side chain of Met311 causes a significant shift of Arg37 (Figure 3 and Supporting Information Figure S2), the “gatekeeper” of the acetate product release channel.³⁴ The shift of Arg37 breaks its hydrogen bonds with the backbone carbonyl groups of Gly303 and Gly305. Thus, product release may be compromised in T311M HDAC8.

Notably, the movement of Arg37 causes the adjacent L1 loop (Leu31–Pro35) to reorganize (Figure 3). This loop is involved in substrate binding through an enzyme–substrate hydrogen bond with Lys33.^{30,31,35} Conformational changes in the L1 loop propagate through to the L2 loop, which is also important for substrate binding. Thus, the T311M mutation may indirectly influence substrate interactions with these loops. Interestingly, these loop movements are sufficiently large to hinder the binding of a second inhibitor molecule in the outer active site cleft, as observed in the wild-type HDAC8–TSA complex (Supporting Information Figure S3).³³

A188T HDAC8. Ala188 is located in helix D, ~18 Å away from the active site Zn²⁺ ion, and is buried in a hydrophobic environment. A188T HDAC8 exhibits 39% residual activity compared with wild-type HDAC8 (Table 1). The structure of the A188T HDAC8–M344 complex is similar to that of the corresponding wild-type HDAC8 complex (rms deviation = 0.41 Å for 357 Cα atoms).³³ However, there are local structural changes in the vicinity of the mutation. The Thr188 hydroxyl group donates a hydrogen bond to the backbone carbonyl of Gly184, which may compromise hydrogen bonding that stabilizes helix D (Figure 4a). Additionally, surrounding hydrophobic residues, especially Phe70, and their associated loops, shift 0.3–0.6 Å to accommodate the larger Thr188 side chain (Supporting Information Figure S4). Subtle structural changes propagate through to adjacent helices, including helix

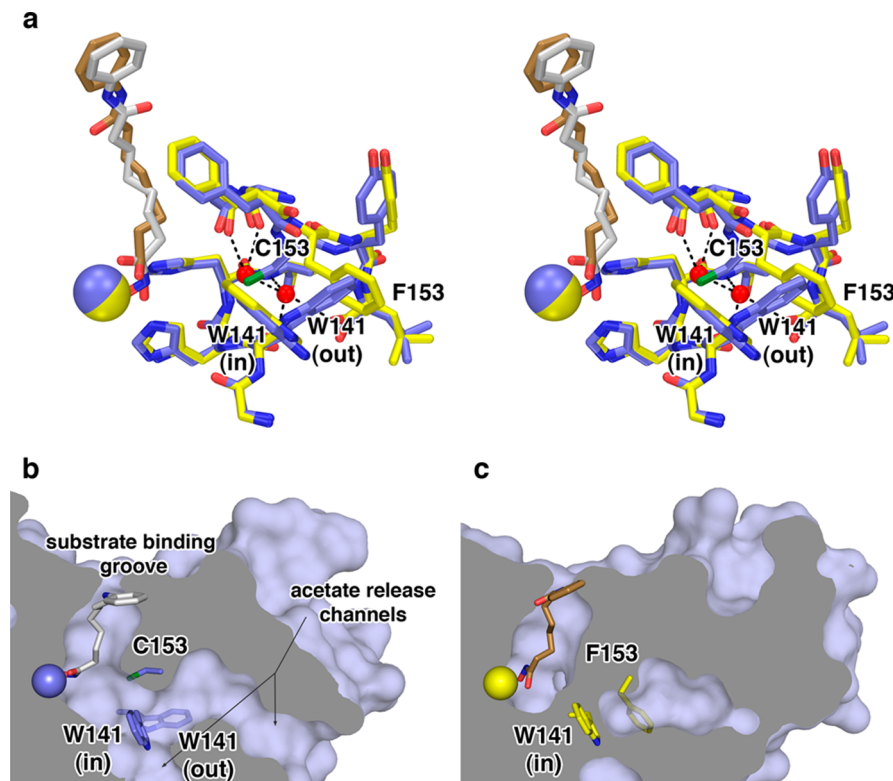


Figure 2. C153F HDAC8. (a) Superimposition of the HDAC8 C153F-SAHA complex (monomer A: C = yellow, N = blue, O = red, S = green, Zn^{2+} = yellow sphere, SAHA = tan) and the wild-type HDAC8-SAHA complex (PDB 1T69, color-coded as above except C = blue, Zn^{2+} = blue sphere, SAHA = gray). Water molecules (red spheres) occupy the space previously occupied by the C153 side chain. The F153 side chain sterically locks W141 in the “in” conformation, whereas W141 is disordered between “in” and “out” conformations in wild-type HDAC8. (b) Cutaway view of the solvent-accessible surface of wild-type HDAC8 shows that the W141 side chain, in the “in” and “out” conformation, respectively, closes and opens the acetate release channels; the surface shown is calculated only for the “out” conformation to illustrate the open channels. (c) Corresponding view of C153F HDAC8 reveals that the acetate release channel is completely blocked because the W141 side chain is sterically locked in the “in” conformation by the C153F mutation. Parenthetically, we note that the L2 loop (E85–H90) is partially disordered in wild-type but not C153F HDAC8, which leads to slight differences in the upper right solvent-accessible surface in b and c.

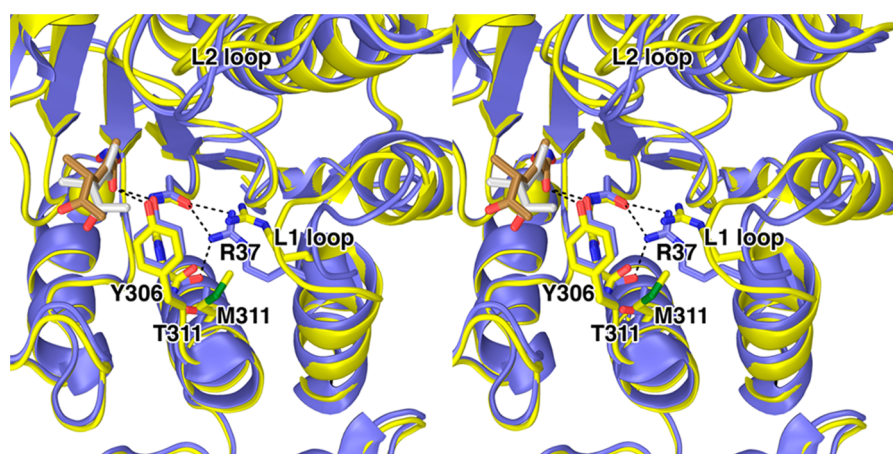


Figure 3. T311M HDAC8. Comparison of the T311M HDAC8-TSA complex (yellow, C = yellow (protein) or tan (TSA), N = blue, O = red, S = green, Zn^{2+} = yellow sphere, monomer A) and the wild-type HDAC8-TSA complex (blue, Zn^{2+} = blue sphere, TSA = gray; PDB 1T64). Hydrogen bonds are indicated by black dashed lines. The aromatic ring of each TSA molecule is omitted for clarity. The T311M mutation causes significant conformational changes in the L1 loop, which in turn are transmitted to the L2 loop. The L1 and L2 loops play a role in substrate binding, so structural changes may compromise this function.

B2, which leads to the L2 loop. The A188T mutation may thus influence substrate binding through the L2 loop.

To enable the study of an intact tetrapeptide assay substrate bound in the active site, we inactivated HDAC8 by making the Y306F mutation;³⁰ the preparation of selected double mutants

bearing this mutation as well as a CdLS mutation allowed us to evaluate the structural consequences of the CdLS mutation on substrate binding. The structure of the A188T/Y306F HDAC8-substrate complex (Figure 4b and Supporting Information Figure S5) is similar to that of the A188T HDAC8-M344

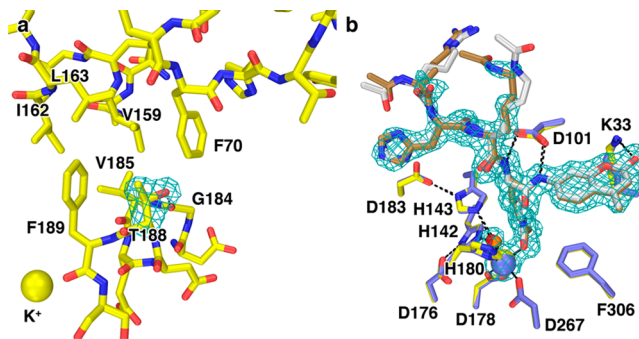


Figure 4. A188T HDAC8. (a) Simulated annealing omit map (contoured at 2.5σ) showing the T188 side chain in the A188T HDAC8-M344 complex (monomer B). Atomic color codes are as follows: C = yellow, N = blue, O = red, K^+ = yellow sphere. The hydrogen bond between the T188 hydroxyl group and the backbone carbonyl of G184 is shown as a black dashed line. (b) Simulated annealing omit map (contoured at 3.0σ) showing the partially disordered tetrapeptide substrate bound in the active site of the A188T/Y306F HDAC8-substrate complex (monomer A). Atomic color codes are as follows: C = yellow (protein) or tan (substrate), N = blue, O = red, Zn^{2+} = yellow sphere, water molecule = red sphere. Metal coordination and hydrogen bond interactions are shown as solid black and dashed black lines, respectively. Also superimposed is the Y306F HDAC8-substrate complex (C = blue (protein) or gray (substrate), Zn^{2+} = blue sphere, water molecule = orange sphere; PDB 2V5W) (for a stereoview, see Supporting Information Figure S5).

complex (rms deviation = 0.37 \AA for 364 $\text{C}\alpha$ atoms). Hydrophobic residues surrounding Thr188 generally maintain their positions in both structures, although structural changes propagating through to helix B2 are attenuated. Even so, the L2 loop is fully ordered in all monomers and adopts a conformation slightly different from that observed in the Y306F HDAC8-substrate complex.³⁰ However, although the tetrapeptide substrate binds in a similar manner to A188T/Y306F HDAC8 and Y306F HDAC8, the substrate is partially disordered in the complex with A188T/Y306F HDAC8: the acetyl-arginine residue is highly disordered in both monomers, and the acetyl-lysine that does not bind to the active site Zn^{2+} ion is partially disordered in monomer A (Figure 4b and Supporting Information Figure S5). Thus, the subtle structural changes caused by the A188T substitution appear to influence substrate binding.

I243N HDAC8. Ile243 is located in helix F, $\sim 18 \text{ \AA}$ away from the active site Zn^{2+} ion, buried in a hydrophobic environment. I243N HDAC8 exhibits 41% activity relative to the wild-type enzyme (Table 1). The structure of the I243N HDAC8-SAHA complex is similar to that of the wild-type HDAC8-SAHA complex³³ (rms deviation = 0.50 \AA for 357 $\text{C}\alpha$ atoms). As shown in Figure 5a, the I243N mutation introduces a polar side chain in the nonpolar protein interior, which is destabilizing. Accordingly, I243N HDAC8 exhibits the most significant decrease in thermostability of the five mutants studied ($\Delta T_m = -9.5 \text{ }^\circ\text{C}$; Table 1). Neighboring residues shift to accommodate Asn243, resulting in a slight shift of neighboring helix H3 (Supporting Information Figure S6). These subtle structural changes may be responsible for the flipped binding conformation of SAHA (Supporting Information Figure S7).

The structure of the I243N/Y306F HDAC8-substrate complex reveals that substrate binding appears to attenuate the slight shift of helix H3, which is not as pronounced as that

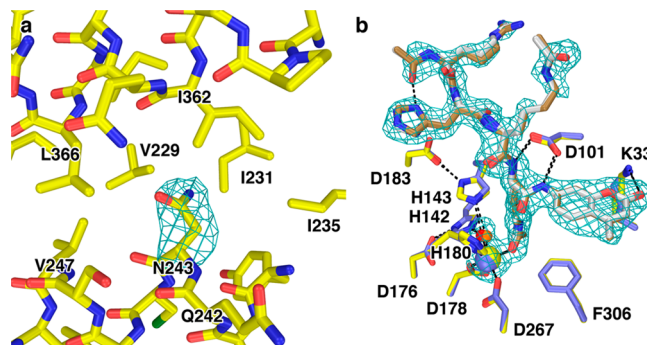


Figure 5. I243N HDAC8. (a) Simulated annealing omit map (contoured at 2.5σ) showing the N243 side chain in the I243N HDAC8-SAHA complex (monomer B). Atomic color codes are as follows: C = yellow, N = blue, O = red, S = green. (b) Comparison of substrate binding in the I243N/Y306F HDAC8-substrate complex (C = yellow (protein) or tan (substrate), N = blue, O = red, Zn^{2+} = yellow sphere, monomer A) and the Y306F HDAC8-substrate complex (C = blue (protein) or gray (substrate), N = blue, O = red, Zn^{2+} = blue sphere) (PDB 2V5W, monomer A). Water molecules are indicated as red or orange spheres, respectively. Metal coordination and hydrogen bond interactions are shown as solid black and dashed black lines, respectively. The simulated annealing omit map (contoured at 3.0σ) shows a nearly fully ordered tetrapeptide substrate bound in the active site of I243N/Y306F HDAC8 (for a stereoview, see Supporting Information Figure S8).

observed in the I243N HDAC8-SAHA complex. The tetrapeptide substrate is fully ordered and it binds similarly to I243N/Y306F HDAC8 and Y306F HDAC8 (Figure 5b and Supporting Information Figure S8).

H334R HDAC8. His334 is located $\sim 25 \text{ \AA}$ away from the active site and is the most distant of the mutants described in this study. Although this residue is located near the protein surface, its imidazole side chain is oriented toward the protein interior, where it hydrogen bonds with a buried water molecule that in turn hydrogen bonds with Tyr340 and the backbone carbonyl of Met40. H334R HDAC8 exhibits 91% residual activity compared with the wild-type enzyme (Table 1), so the functional consequences of this mutation are minimal. Although the structure of the H334R HDAC8-M344 complex is similar overall to that of the wild-type HDAC8-M344 complex³³ (rms deviation = 0.45 \AA for 357 $\text{C}\alpha$ atoms), significant local structural changes are triggered by the mutation (Figure 6). The larger guanidinium side chain of Arg334 cannot fit in the space formerly occupied by His334, so the polypeptide backbone flips so that Arg334 is oriented toward solvent. In turn, adjacent residue Asp333 flips toward the protein interior to hydrogen bond with Ser43, the backbone NH groups of Glu335 and Phe336, and the aforementioned buried water molecule.

The structure of the H334R/Y306F HDAC8-substrate complex is very similar to that of the H334R HDAC8-M344 complex, with an rms deviation of 0.27 \AA for 365 $\text{C}\alpha$ atoms. The tetrapeptide substrate is fully ordered in the H334R/Y306F HDAC8-substrate complex and adopts a conformation very similar to that observed in the Y306F HDAC8-substrate complex (Supporting Information Figures S9 and S10). However, Trp141 and Tyr111 each exclusively adopt “in” conformations, so substrate binding appears to stabilize the conformations of these residues. In certain wild-type and H334R HDAC8-inhibitor complexes, these residues are disordered between “in” and “out” conformations; the “out”

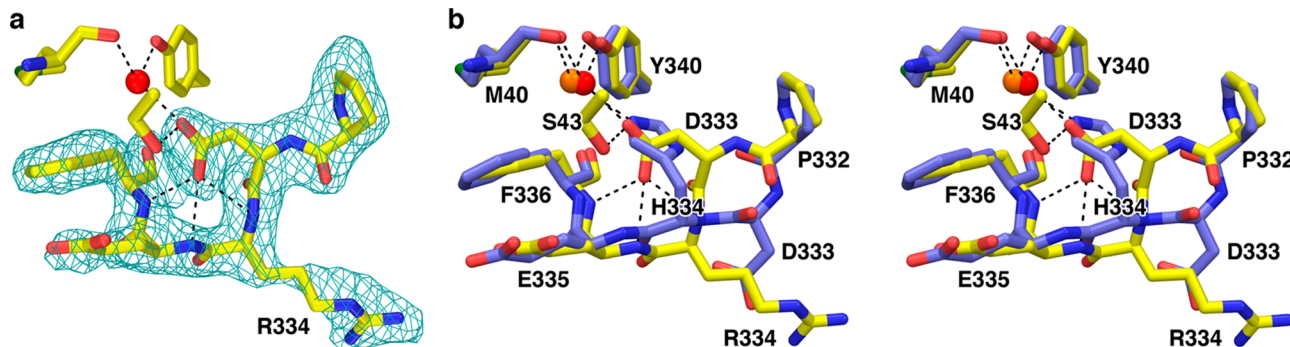


Figure 6. H334R HDAC8. (a) Simulated annealing omit map (contoured at 2.0σ) showing the R334 side chain in the H334R HDAC8-M344 complex. Atomic color codes are as follows: C = yellow, N = blue, O = red, S = green, water molecule = red sphere. (b) Superposition of the H334R HDAC8-M344 complex (color-coded as in part a) and the wild-type HDAC8-TSA complex (color-coded similarly, except C = blue and water molecule = orange sphere; PDB 1T64). Hydrogen bond interactions are shown as dashed black lines. The H334R substitution causes a reorganization of the loop containing this residue.

conformation of Trp141 is required to facilitate acetate departure through product release channels during catalysis.

Thermostability of HDAC8 Mutants. All CdLS HDAC8 mutants studied exhibit diminished thermostability compared with the wild-type enzyme (Table 1). Thermostability is most significantly compromised by the I243N mutation with $\Delta T_m = -9.5$ °C, and least compromised by the C153F mutation with $\Delta T_m = -1.9$ °C. As expected, the binding of M344 increases the melting temperature of HDAC8 and its mutants.

Diminished thermostability can significantly amplify the biological consequences of compromised catalytic function. Even though wild-type HDAC8 exhibits a 36% loss of activity after 15 min at 37 °C, the C153F, A188T, H334R, T311M, and I243N HDAC8 mutants exhibit 41%, 49%, 80%, 81%, and 85% activity losses, respectively (Supporting Information Figure S11). Interestingly, although wild-type and H334R HDAC8s exhibit nearly identical catalytic activities, H334R HDAC8 is much less thermostable than the wild-type enzyme ($\Delta T_m = -7.0$ °C) and exhibits more than double the activity loss after incubation for 15 min at 37 °C.

Rescue of Catalysis by an N-Acylthiourea Activator. N-acylthiourea derivatives were recently reported by Singh and colleagues to act as selective activators of HDAC8.³² We evaluated N-(phenylcarbamothioyl)benzamide (TM-2-51) with CdLS HDAC8 mutants and found that it could modestly activate catalytic activity in a dose-dependent fashion (Figure 7, Supporting Information Table S3). The activation profile for each CdLS mutant is similar to that of the wild-type enzyme, with 2–3 fold activation observed for all of the mutants except for C153F HDAC8. Notably, the compromised catalytic activities of certain mutants, such as A188T HDAC8 and I243N HDAC8, can be restored to wild-type levels. We hypothesize that the activator binds to the enzyme and somehow compensates for defects in structure or stability caused by the mutations.

Structure–Function Relationships and Clinical Implications. X-ray crystal structures of HDAC8 mutants identified in children diagnosed with CdLS correlate with catalytic activity and thermostability measurements to establish the molecular basis of a newly discovered cause of CdLS. Strictly conserved (Ala188, Cys153) or highly conserved (Ile243, Thr311, and His334) residues are mutated in CdLS, and the severity of compromised catalysis tends to correlate with proximity to the active site. For example, Cys153 is closest to the active site of the five residues studied, and C153F HDAC8 exhibits only 2%

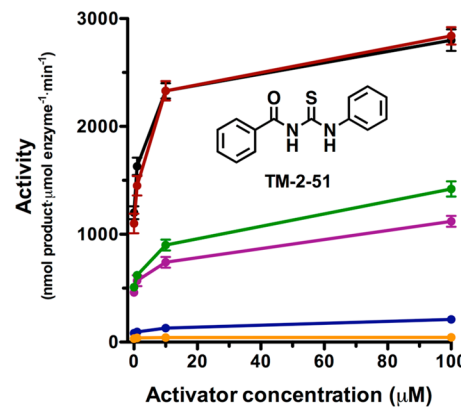


Figure 7. Dose-dependent activation of HDAC8 activity by TM-2-51. Color-code: wild-type = black, C153F = orange, A188T = purple, I243N = green, T311M = blue, H334R = red; data are reported in tabular form in Supporting Information Table S3.

residual activity. The crystal structure of this mutant reveals that the mutation causes conformational changes in Trp141 such that both Phe153 and Trp141 permanently block internal channels that enable product release. Similarly, the T311M mutation is also close to the active site, and this mutant exhibits only 6% residual activity. This mutation causes conformational changes in nearby residue Arg37, which serves as a “gatekeeper” for the acetate product release channels.

In contrast, the H334R mutation is most distant from the active site and has only a minor effect on catalysis (91% residual activity). Although significant structural changes are triggered by this mutation in a loop ~25 Å from the active site, these changes do not perturb the structure of the active site or the enzyme–substrate complex. However, the thermostability of H334R HDAC8 is significantly compromised. Thus, compromised biological function of HDAC8 mutants in CdLS can result from diminished thermostability as well as compromised catalytic activity.

Direct correlation of clinical severity with the activity of HDAC8 mutants is difficult, because of the X-linked nature of the *HDAC8* gene, which results in the random inactivation of this gene in various tissues in females. However, some modest correlations appear to be evident. For example, patients diagnosed with the H334R mutation have a relatively moderate phenotype. This is likely a consequence of only a very mild reduction in catalytic activity coupled with a significant decrease

in thermostability—none of the H334R patients resemble the severe, classic CdLS phenotype. In comparison, a girl with a T311M mutation has a fairly classic CdLS phenotype, consistent with significant reductions in both catalytic activity and thermostability. A possible correlation between HDAC8 mutation and CdLS phenotype is further supported by the observation that the only patient with an H180R mutation has died. His180 plays a crucial role in catalysis and thermostability by coordinating to the active site Zn²⁺ ion; the H180R mutation destroys the Zn²⁺ binding site and abolishes catalytic activity.^{28,29} Thus, to some degree, the apparent severity of symptoms presented by children diagnosed with CdLS appears to correlate with the severity of compromised catalysis and/or diminished thermostability of HDAC8 mutants.

It is noteworthy that catalytic activity can be rescued in some of the HDAC8 mutants by a small-molecule activator. Ultimately, such an activator could potentially be useful in the therapeutic management of CdLS. While we have been unsuccessful to date in preparing a crystalline HDAC8-substrate-activator complex, we hypothesize that the activator might somehow stabilize the protein conformation that accommodates substrate binding. Even so, some of the most inactive mutants, such as C153F HDAC8, are so badly compromised that an activator cannot easily rescue catalysis. In this mutant, for example, the activator is probably unable to open up the blocked product release channel, so the activation is minimal. Thus, the potential therapeutic efficacy of an HDAC8 activator in the management of CdLS would depend on the specific HDAC8 mutation involved.

While pre-existing physical deformities would not be reversed in a CdLS patient by the administration of an HDAC8 activator, the rescue of catalytic activity in a mutant enzyme could potentially attenuate the progression of development-related deformities and neurocognitive impairment in a patient diagnosed with an HDAC8 mutation. Hence, this possible therapeutic approach merits further exploration, and our results in this regard will be reported in due course.

METHODS

Mutations in human HDAC8 were introduced into the previously described HDAC8-6His-pET20b construct³¹ using QuikChange site-directed mutagenesis (Agilent Genomics) as detailed in the Supporting Information. The Fluor-de-Lys tetrapeptide assay substrate Ac-Arg-His-Lys(Ac)-Lys(Ac)-aminomethylcoumarin (BML-KI178-0005, Enzo Life Sciences)³⁶ was used to measure the catalytic activities of HDAC8 mutants, as previously described.^{28,29} Heat inactivation studies were performed by equilibrating 10 μM enzyme stock solutions at 37 °C for 15, 30, or 60 min, after which enzyme solutions were diluted to the desired concentration for activity assay. Activity assays after heat inactivation were performed at 25 °C as described;^{28,29} activity assays with the HDAC8 activator³² TM-2-51 were performed in a similar manner as detailed in the Supporting Information.

The thermostabilities of HDAC8 mutants were assessed using a thermal shift assay³⁷ as outlined in the Supporting Information. This assay utilizes SYPRO orange dye (S6650, Life Technologies), which associates with the exposed hydrophobic surfaces of an unfolded protein and fluoresces at λ_{em} = 615 nm. Melting temperatures (T_m) were designated as the inflection point in the fluorescence curve as a function of temperature.

Crystals of HDAC8 mutant-inhibitor and -substrate complexes were prepared by cocrystallization at 21 or 4 °C in sitting drops using the vapor diffusion method, as previously described.³¹ Complete details for the crystallization of each complex are reported in the Supporting Information, and the chemical structure of each inhibitor is illustrated

in Supporting Information Figure S12. All X-ray diffraction data were collected on beamline X29 at the National Synchrotron Light Source (NSLS, Brookhaven National Laboratory). Data were collected at resolutions ranging 1.76–2.88 Å and were indexed, integrated, and scaled using HKL2000.³⁸ Crystal structures were solved by molecular replacement and refined using routines implemented in PHENIX.³⁹ Complete details are provided in the Supporting Information, and data collection and refinement statistics are recorded in Supporting Information Table S2.

ASSOCIATED CONTENT

Supporting Information

Additional methods, figures, and tables. This material is available free of charge via the Internet at <http://pubs.acs.org>.

Accession Codes

The atomic coordinates and the crystallographic structure factors of HDAC8 mutants C153F, A188T, I243N, T311M, H334R, A188T/Y306F, I243N/Y306F, and H334R/Y306F have been deposited in the Protein Data Bank (www.rcsb.org) with accession codes 4QA0, 4QA1, 4QA2, 4QA3, 4QA4, 4QA5, 4QA6, and 4QA7, respectively.

AUTHOR INFORMATION

Corresponding Author

*Email: chris@sas.upenn.edu.

Notes

The authors declare no competing financial interest.

ACKNOWLEDGMENTS

We thank the Research Foundation of the University of Pennsylvania, the Doris Duke Charitable Foundation, the Vagelos Program in Molecular Life Sciences, and the National Institutes of Health (NIH) for grants GM49758 and K08HD055488 in support of this research. Additionally, we thank G. Cook, R. Singh, T. Mandal, and D.K. Srivastava for the generous gift of TM-2-51, and K. Bethoney and A. Lebedev for helpful discussions. Finally, we thank the NSLS for access to beamline X29 for X-ray crystallographic data collection.

ABBREVIATIONS

CdLS, Cornelia de Lange Syndrome; HDAC8, histone deacetylase 8; M344, 4-(dimethylamino)-N-[7-(hydroxyamino)-7-oxoheptyl]benzamide; PDB, Protein Data Bank; SAHA, suberoylanilide hydroxamic acid; TSA, trichostatin A

REFERENCES

- (1) Losada, A. (2008) The regulation of sister chromatid cohesion. *Biochim. Biophys. Acta* 1786, 41–48.
- (2) Nasmyth, K., and Haering, C. H. (2009) Cohesin: Its roles and mechanisms. *Annu. Rev. Genet.* 43, 525–558.
- (3) Gruber, S., Haering, C. H., and Nasmyth, K. (2003) Chromosomal cohesin forms a ring. *Cell* 112, 765–777.
- (4) Remeseiro, S., and Losada, A. (2013) Cohesin, a chromatin engagement ring. *Curr. Opin. Cell Biol.* 25, 63–71.
- (5) McNairn, A. J., and Gerton, J. L. (2008) Cohesinopathies: One ring, many obligations. *Mutat. Res.* 647, 103–111.
- (6) Barbero, J. L. (2013) Genetic basis of cohesinopathies. *Appl. Clin. Genet.* 6, 15–23.
- (7) van der Lelij, P., Chrzanowska, K. H., Godthelp, B. C., Rooimans, M. A., Oostra, A. B., Stumm, M., Zdzienicka, M. Z., Joenje, H., and de Winter, J. P. (2010) Warsaw breakage syndrome, a cohesinopathy associated with mutations in the XPD helicase family member DDX11/Chlrl. *Am. J. Hum. Genet.* 86, 262–266.

- (8) Liu, J., and Krantz, I. D. (2009) Cornelia de Lange syndrome, cohesin, and beyond. *Clin. Genet.* 76, 303–314.
- (9) Dorsett, D., and Krantz, I. D. (2009) On the molecular etiology of Cornelia de Lange syndrome. *Ann. N.Y. Acad. Sci.* 1151, 22–37.
- (10) Ciosk, R., Shirayama, M., Shevchenko, A., Tanaka, T., Toth, A., Shevchenko, A., and Nasmyth, K. (2000) Cohesin's binding to chromosomes depends on a separate complex consisting of Scc2 and Scc4 proteins. *Mol. Cell* 5, 243–254.
- (11) Takahashi, T. S., Yiu, P., Chou, M. F., Gygi, S., and Walter, J. C. (2004) Recruitment of Xenopus Scc2 and cohesin to chromatin requires the pre-replication complex. *Nat. Cell Biol.* 6, 991–996.
- (12) Krantz, I. D., McCallum, J., DeScipio, C., Kaur, M., Gillis, L. A., Yaeger, D., Jukofsky, L., Wasserman, N., Bottani, A., Morris, C. A., Nowaczky, M. J., Toriello, H., Bamshad, M. J., Carey, J. C., Rappaport, E., Kawauchi, S., Lander, A. D., Calof, A. L., Li, H. H., Devoto, M., and Jackson, L. G. (2004) Cornelia de Lange syndrome is caused by mutations in NIPBL, the human homolog of *Drosophila melanogaster* Nipped-B. *Nat. Genet.* 36, 631–635.
- (13) Tonkin, E. T., Wang, T. J., Lisgo, S., Bamshad, M. J., and Strachan, T. (2004) NIPBL, encoding a homolog of fungal Scc2-type sister chromatid cohesion proteins and fly Nipped-B, is mutated in Cornelia de Lange syndrome. *Nat. Genet.* 36, 636–641.
- (14) Gillis, L. A., McCallum, J., Kaur, M., DeScipio, C., Yaeger, D., Mariani, A., Kline, A. D., Li, H. H., Devoto, M., Jackson, L. G., and Krantz, I. D. (2004) NIPBL mutational analysis in 120 individuals with Cornelia de Lange syndrome and evaluation of genotype–phenotype correlations. *Am. J. Hum. Genet.* 75, 610–623.
- (15) Deardorff, M. A., Kaur, M., Yaeger, D., Rampuria, A., Korolev, S., Pie, J., Gil-Rodríguez, C., Arnedo, M., Loey, B., Kline, A. D., Wilson, M., Lillquist, K., Siu, V., Ramos, F. J., Musio, A., Jackson, L. S., Dorsett, D., and Krantz, I. D. (2007) Mutations in cohesin complex members SMC3 and SMC1A cause a mild variant of Cornelia de Lange syndrome with predominant mental retardation. *Am. J. Hum. Genet.* 80, 485–494.
- (16) Deardorff, M. A., Wilde, J. J., Albrecht, M., Dickinson, E., Tennstedt, S., Braunholz, D., Mönnich, M., Yan, Y., Xu, W., Gil-Rodríguez, M. C., Clark, D., Hakonarson, H., Halbach, S., Michelis, L. D., Rampuria, A., Rossier, E., Spranger, S., Van Maldergem, L., Lynch, S. A., Gillessen-Kaesbach, G., Lüdecke, H. J., Ramsay, R. G., McKay, M. J., Krantz, I. D., Xu, H., Horsfield, J. A., and Kaiser, F. J. (2012) RAD21 mutations cause a human cohesinopathy. *Am. J. Hum. Genet.* 90, 1014–1027.
- (17) Zhang, J., Shi, X., Li, Y., Kim, B. J., Jia, J., Huang, Z., Yang, T., Fu, X., Jung, S. Y., Wang, Y., Zhang, P., Kim, S. T., Pan, X., and Qin, J. (2008) Acetylation of Smc3 by Eco1 is required for S phase sister chromatid cohesion in both human and yeast. *Mol. Cell* 31, 143–151.
- (18) Ben-Shahar, T. R., Heeger, S., Lehane, C., East, P., Flynn, H., Skehel, M., and Uhlmann, F. (2008) Eco1-dependent cohesin acetylation during establishment of sister chromatid cohesion. *Science* 321, 563–566.
- (19) Unal, E., Heidinger-Pauli, J. M., Kim, W., Guacci, V., Onn, I., Gygi, S. P., and Koshland, D. E. (2008) A molecular determinant for the establishment of sister chromatid cohesion. *Science* 321, 566–569.
- (20) Beckouët, F., Hu, B., Roig, M. B., Sutani, T., Komata, M., Uluocak, P., Katis, V. L., Shirahige, K., and Nasmyth, K. (2010) An Smc3 acetylation cycle is essential for establishment of sister chromatid cohesion. *Mol. Cell* 39, 689–699.
- (21) Uhlmann, F., Lottspeich, F., and Nasmyth, K. (1999) Sister-chromatid separation at anaphase onset is promoted by cleavage of the cohesin subunit Scc1. *Nature* 400, 37–42.
- (22) Xiong, B., Lu, S., and Gerton, J. L. (2010) Hos1 is a lysine deacetylase for the Smc3 subunit of cohesin. *Curr. Biol.* 20, 1660–1665.
- (23) Borges, V., Lehane, C., Lopez-Serra, L., Flynn, H., Skehel, M., Ben-Shahar, T. R., and Uhlmann, F. (2010) Hos1 deacetylates Smc3 to close the cohesin acetylation cycle. *Mol. Cell* 39, 677–688.
- (24) Yang, X. J., and Seto, E. (2008) The Rpd3/Hda1 family of lysine deacetylases: From bacteria and yeast to mice and men. *Nat. Rev. Mol. Cell Biol.* 9, 206–218.
- (25) Lombardi, P. M., Cole, K. E., Dowling, D. P., and Christianson, D. W. (2011) Structure, mechanism, and inhibition of histone deacetylases and related metalloenzymes. *Curr. Opin. Struct. Biol.* 21, 735–743.
- (26) Wolfson, N. A., Pitcairn, C. A., and Fierke, C. A. (2013) HDAC8 substrates: Histones and beyond. *Biopolymers* 99, 112–126.
- (27) de Ruijter, A. J., van Gennip, A. H., Caron, H. N., Kemp, S., and van Kuilenburg, A. B. (2003) Histone deacetylases (HDACs): Characterization of the classical HDAC family. *Biochem. J.* 370, 737–749.
- (28) Deardorff, M. A., Bando, M., Nakato, R., Watrin, E., Itoh, T., Minamino, M., Saitoh, K., Komata, M., Katou, Y., Clark, D., Cole, K. E., De Baere, E., Decroos, C., Di Donato, N., Ernst, S., Francey, L. J., Gyftodimou, Y., Hirashima, K., Hullings, M., Ishikawa, Y., Jaulin, C., Kaur, M., Kiyono, T., Lombardi, P. M., Magnaghi-Jaulin, L., Mortier, G. R., Nozaki, N., Petersen, M. B., Seimiya, H., Siu, V. M., Suzuki, Y., Takagaki, K., Wilde, J. J., Willems, P. J., Prigent, C., Gillessen-Kaesbach, G., Christianson, D. W., Kaiser, F. J., Jackson, L. G., Hirota, T., Krantz, I. D., and Shirahige, K. (2012) HDAC8 mutations in Cornelia de Lange syndrome affect the cohesin acetylation cycle. *Nature* 489, 313–317.
- (29) Kaiser, F. J., Ansari, M., Braunholz, D., Gil-Rodríguez, M. C., Decroos, C., Wilde, J. J., Fincher, C. T., Kaur, M., Bando, M., Amor, D. J., Atwal, P. S., Bahlo, M., Bowman, C. M., Bradley, J. J., Brunner, H. G., Clark, D., Del Campo, M., Di Donato, N., Diakumis, P., Dubbs, H., Dymant, D. A., Eckhold, J., Ernst, S., Ferreira, J. C., Francey, L. J., Gehlken, U., Guillén-Navarro, E., Gyftodimou, Y., Hall, B. D., Hennekam, R., Hudgins, L., Hullings, M., Hunter, J. M., Yntema, H., Innes, A. M., Kline, A. D., Krumina, Z., Lee, H., Leppig, K., Lynch, S. A., Mallozzi, M. B., Mannini, L., McKee, S., Mehta, S. G., Micule, I., Care4Rare Canada Consortium, Mohammed, S., Moran, E., Mortier, G. R., Moser, J.-A. S., Noon, S. E., Nozaki, N., Nunes, L., Pappas, J. G., Penney, L. S., Pérez-Aytés, A., Petersen, M. B., Puisac, B., Revencu, N., Roeder, E., Saitta, S., Scheuerle, A. E., Schindeler, K. L., Siu, V. M., Stark, Z., Strom, S. P., Thiese, H., Vater, I., Willems, P., Williamson, K., Wilson, L. C., University of Washington Center for Mendelian Genomics, Hakonarson, H., Quintero-Rivera, F., Wierzb, J., Musio, A., Gillessen-Kaesbach, G., Ramos, F. J., Jackson, L. G., Shirahige, K., Pié, J., Christianson, D. W., Krantz, I. D., Fitzpatrick, D. R., and Deardorff, M. A. (2014) Loss of function HDAC8 mutations cause a phenotypic spectrum of Cornelia de Lange Syndrome-like features, ocular hypertelorism, large fontanelle, and X-linked inheritance. *Hum. Mol. Genet.* 23, 2888–2900.
- (30) Vannini, A., Volpari, C., Gallinari, P., Jones, P., Mattu, M., Carfi, A., De Francesco, R., Steinkühler, C., and Di Marco, S. (2007) Substrate binding to histone deacetylases as shown by the crystal structure of the HDAC8-substrate complex. *EMBO Rep.* 8, 879–884.
- (31) Dowling, D. P., Gantt, S. L., Gattis, S. G., Fierke, C. A., and Christianson, D. W. (2008) Structural studies of human histone deacetylase 8 and its site-specific variants complexed with substrate and inhibitors. *Biochemistry* 47, 13554–13563.
- (32) Singh, R. K., Mandal, T., Balsubramanian, N., Viaene, T., Leedahl, T., Sule, N., Cook, G., and Srivastava, D. K. (2011) Histone deacetylase activators: N-acetylthioureas serve as highly potent and isozyme selective activators for human histone deacetylase-8 on a fluorescent substrate. *Bioorg. Med. Chem. Lett.* 21, 5920–5923.
- (33) Somoza, J. R., Skene, R. J., Katz, B. A., Mol, C., Ho, J. D., Jennings, A. J., Luong, C., Arvai, A., Buggy, J. J., Chi, E., Tang, J., Sang, B. C., Verner, E., Wynands, R., Leahy, E. M., Dougan, D. R., Snell, G., Navre, M., Knuth, M. W., Swanson, R. V., McRee, D. E., and Tari, L. W. (2004) Structural snapshots of human HDAC8 provide insights into the class I histone deacetylases. *Structure* 12, 1325–1334.
- (34) Haider, S., Joseph, C. G., Neidle, S., Fierke, C. A., and Fuchter, M. J. (2011) On the function of the internal cavity of histone deacetylase protein 8: R37 is a crucial residue for catalysis. *Bioorg. Med. Chem. Lett.* 21, 2129–2132.
- (35) Kunze, M. B., Wright, D. W., Werbeck, N. D., Kirkpatrick, J., Coveney, P. V., and Hansen, D. F. (2013) Loop interactions and

dynamics tune the enzymatic activity of the human histone deacetylase 8. *J. Am. Chem. Soc.* 135, 17862–17868.

(36) Wegener, D., Wirsching, F., Riester, D., and Schwienhorst, A. (2003) A fluorogenic histone deacetylase assay well suited for high-throughput activity screening. *Chem. Biol.* 10, 61–68.

(37) Niesen, F. H., Berglund, H., and Vedadi, M. (2007) The use of differential scanning fluorimetry to detect ligand interactions that promote protein stability. *Nat. Protoc.* 2, 2212–2221.

(38) Otwinowski, Z., and Minor, W. (1997) Processing of X-ray diffraction data collected in oscillation mode. *Methods Enzymol.* 276, 307–326.

(39) Adams, P. D., Afonine, P. V., Bunkóczki, G., Chen, V. B., Davis, I. W., Echols, N., Headd, J. J., Hung, L. W., Kapral, G. J., Gross-Kunstleve, R. W., McCoy, A. J., Moriarty, N. W., Oeffner, R., Read, R. J., Richardson, D. C., Richardson, J. S., Terwilliger, T. C., and Zwart, P. H. (2010) PHENIX: A comprehensive Python-based system for macromolecular structure solution. *Acta Crystallogr. D66*, 213–221.